ANL/NSE-20/48

Nek5000 Developments in Support of Industry and the NRC

Nuclear Science and Engineering Division

About Argonne National Laboratory

Argonne is a U.S. Department of Energy laboratory managed by UChicago Argonne, LLC under contract DE-AC02-06CH11357. The Laboratory's main facility is outside Chicago, at 9700 South Cass Avenue, Argonne, Illinois 60439. For information about Argonne and its pioneering science and technology programs, see www.anl.gov.

ANL/NSE-20/48

Nek5000 Developments in Support of Industry and the NRC

prepared by

Dillon Shaver[1], Aleks Obabko[2], Ananias Tomboulides[3], Victor Coppo-Leite[4,1], Yu-Hsiang Lan[3], MiSun Min[3], Paul Fischer[5,3], and Christopher Boyd[6]

[1]Nuclear Science and Engineering Division, Argonne National Laboratory
[2]Computational Science Division, Argonne National Laboratory
[3]Mathematics and Computer Science Division, Argonne National Laboratory
[4]Department of Mechanical and Nuclear Engineering, Pennsylvania State University
[5]Department of Mechanical Science and Engineering and Department of Computer Science, University of Illinois at Urbana-Champaign
[6]U.S. Nuclear Regulatory Commission

September 30, 2020

Contents

Abstract

This year, the Nuclear Energy Advanced Modeling Simulation program (NEAMS) thermal-hydraulics verification and validation (V&V) work has focused in three areas of Nek5000 V&V-driven development.

First, in a close collaborative effort with the U. S. Nuclear Regulatory Commission (NRC) staff, we have continued V&V efforts for the HYMERES-2 project using the OECD/NEA sponsored testing in the PSI PANDA facility. This year's focus of ANL-NRC collaboration involves Nek5000 setups and validation for a range of problems relevant to and including the HYMERES-2 benchmark from PSI. The primary outcome of this year efforts is a more efficient geometry and inlet modeling simplification after a careful sensitivity study of the inlet profiles and pipe geometries. The resulting modeling choice of a short recycling/fully-developed turbulent inlet is within the experimental uncertainty estimate. This finding simplifies the next step of the cross-V&V HYMERES-2 project. In addition, the ANL team continue to provide assistance to the NRC staff in the form of Nek5000 application support in general and on the use of the HPC platforms of ALCF and INL in particular. This supports the NRC's assessment of Nek5000 for use with the NRC Blue CRAB code suite.

Second, we have implemented and tested more robust model of URANS, namely the $k - \tau$ model, a variant of the k-ω model, along with other improvements to RANS Nek5000 modeling in general. Because of its demonstrated robustness and stability, the $k - \tau$ model is the only RANS model that has been implemented in the new GPU version of the Nek5000 code, nekRS.

Lastly, we report the initial implementation of Jacobian-free Newton Krylov approach to the direct Newton method for steady fluid solvers aimed at acceleration of RANS modeling and at IC improvement for LES campaigns.

Also leveraging the Exascale Computing Project (ECP) ANL/CEED & SMR team's software development effort to support NEAMS problems at large scale of the advanced computing architectures, NekRS, a GPU variant of Nek5000, built on top of kernels from libParanumal using OCCA for portability, has been successfully run on the full system of Summit (4608 nodes, 27648 GPUs).

1 Introduction

This year, the Nuclear Energy Advanced Modeling Simulation program (NEAMS) thermal-hydraulics report for Nek5000 [1] verification and validation (V&V) -driven development focuses on three areas of code application and improvement. First, we continue assisting the U. S. Nuclear Regulatory Commission (NRC) staff with Nek5000 setups and validation for the Hydrogen Mitigation Experiments for REactor Safety (HYMERES-2) benchmark. Second, we have implemented and tested a more robust unsteady Reynolds-averaged Navier-Stokes (URANS) model, namely the $k-\tau$ model, along with other improvements to RANS modeling in Nek in general. Lastly, we report the initial implementation of Jacobian-free Newton Krylov approach to the direct Newton method for steady fluid solvers aimed at acceleration of RANS modeling and at initial condition improvement for large eddy simulations (LES).

With the U. S. nuclear industry on the cusp of deploying the next-generation of power reactors, the NEAMS program is charged with providing the next-generation of modeling and simulation tools. The objective of this work is to assess capabilities in addressing the needs that have been identified as important to both the DOE-NE Advanced Reactor Technologies program (ART) and the nuclear industry. The focus here is on Nek5000, an open-source, highly scalable computational fluid dynamics (CFD) code based on the spectral element method. Nek5000 has traditionally been used to provide accurate reference solutions produced with its high-fidelity capability, typically LES, that could be further used for benchmarking and improving uncertainty estimation for lower-fidelity, faster-turn-around approaches. By building on that pedigree, this work aims to extend the capabilities of Nek5000 to make it more practical for use on problems of relevance to the industry and the NRC.

In a close collaborative effort with the NRC staff, we have continued V&V activity using the Nuclear Energy Agency of the Organization for Economic Co-operation and Development (OECD/NEA) sponsored testing in the PANDA facility. Located at the Paul Scherrer Institute (PSI) in Switzerland, the PANDA facility is a multi-compartment, large-scale thermal-hydraulics test rig that has been used in numerous tests and benchmarks. Recent tests have been focused on providing data for validation of codes for prediction of distribution of buoyant gases including hydrogen during Fukushima-related accident events. Data from these tests including HYMERES-2 measurements has been used as the basis for comparison with CFD results using URANS and LES models in Nek5000.

Last year, the initial meshing and preliminary LES tests kicked off the ANL-NRC collaboration. This collaboration is directly supporting the longer term goals of the NRC related to the improvement of fast lower-fidelity fast-turn-around URANS based turbulence modeling capabilities. In particular, the current model improvement effort is focused on validating against erosion of an air-helium stratified layer as investigated using the previous OECD/NEA PANDA benchmark [2, 3] and current HYMERES-2 project.

The primary focus of this year's efforts of the collaboration was in modeling the benchmark inlet conditions. It was determined that they are sensitive to simplifications in the meshing, geometry, and the upstream level of turbulence. These have implications on the computational efficiency, and thus time-to-solution of the full benchmark geometry problem. In addition, the ANL team has

continued to provide assistance to the NRC staff in the form of Nek5000 application support during the NRC's assessment of the solver usage to support the NRC's Comprehensive Reactor Analysis Bundle (CRAB) code suite.

Another area of the V&V-driven development of Nek5000 is improvement of URANS implementation in the code. Several of the applications of interest to NEAMS can be addressed through RANS modeling. The RANS models currently implemented in Nek5000 are based on the $k-\omega$ model[4]. A significant development during the past year was the implementation and testing of the $k-\tau$ model, which was originally developed by Kalitzin et al.[5, 6] as an alternative implementation of the standard $k-\omega$ model. In contrast to the original model, in which the ω equation contains terms that become singular close to walls, all terms in the k and τ equations reach a finite limit which facilitates their numerical implementation. Moreover, this model does not rely on the wall-distance function or its derivatives.

We investigated and tested various ways to increase the stability, accuracy and robustness of our RANS approaches in order to be able to use larger timesteps by treating several source terms implicitly. This was achieved without any increase of the computational cost. In a separate, on-going effort we are developing the models by extending them to support steady-state solvers with an overall objective to accelerate convergence for turbulent flows in complex geometries. We will continue to develop these solvers to make them effective for production-level simulations at scale. Extensive verification and validation tests of the models were performed for turbulent channel flow, flow past a backward-facing step, as well as external flows, such as flow past a wind turbine blade and the NACA0012 airfoil at various angles of attack. Note that in the latter problem, we have leveraged the support of the Exascale Computing Project (ECP). Due to its demonstrated robustness and stability, the $k-\tau$ model was also implemented in the new GPU version of the Nek5000 code, called nekRS.

We also report on the progress for Nek5000 implementation of direct Newton method for steady fluid solvers using the exact Jacobian formulation. We consider pressure-split preconditioning based on P_N-P_{N-2} projector onto divergence-free space, which will provide a clear path to preconditioning. Once this approach is validated, it will be extensible to the P_N-P_N formulation. This method will be used to accelerate RANS steady state solutions and avoid more expensive time-stepping through URANS in order to reach them. Another potential benefit of RANS steady state solver is a possibility to accelerate and improve initial conditions for LES runs. Note that here also we have leveraged the support of ECP.

The report is organized as follows. Section 2 describes the NRC-ANL collaborative work on Nek5000 application to the OECD/NEA HYMERES-2 relevant geometries. The URANS implementation improvements in Nek5000 are described in Section 3 while Section 4 reports initial implementation of steady state solver in the code. We conclude in Section 5 with a brief summary and outline of the (near) future work.

2 NRC Support

In support of the three-dimensional severe accident safety analyses in nuclear power plants and its improvements, the U. S. NRC is involved with the OECD/NEA HYMERES-2 project which includes high fidelity testing of erosion processes in a layer of helium flow from vertical jets and around obstacles. In close collaboration of ANL with U. S. NRC staff, we have continued validation efforts using the PANDA facility. The experiments performed at this facility include the 2014 OECD/NEA–PSI benchmark which concluded with the CFD For Nuclear Reactor Safety (CFD4NRS-5) workshop at ETH in Zurich. The latter benchmark is aimed at assessment of CFD code maturity and applicability to prediction of Fukushima accident events. These are mimicked in a gradual erosion of an initially stratified air-helium layer by a turbulent round jet consisting primarily of air. Mole fraction and temperature readings were taken at various points throughout the domain to record the erosion behavior, and mean and RMS velocity profiles were averaged over a long transient time. These data were the basis for comparison with CFD results from URANS and LES using Nek5000 and other codes [2, 3].

The turbulent jet erosion of a stratified air-helium layer acts as a surrogate problem used to validate post-Fukushima containment thermal hydraulics and gaseous mixing predictive models. This important problem for nuclear reactor safety is hindered by the challenges of a huge range of modeling scales, transition from forced to buoyancy driven flow with and without obstacles, and the turbulent mixing and erosion of a significantly stratified layer. In particular, the current focus of model improvement involves acquiring the validated reference solution of a stratified layer where the erosion processes like the ones observed in OECD/NEA PANDA benchmark and HYMERES-2 project deviate substantially from the common isotropic turbulence assumption used in lower-fidelity CFD turbulence models and in reduced order/dimensionality models.

This stage of the tests uses a single phase fluid while other variants of the tests will include a mixture of steam near saturation temperature with phase changes. The validation and development work will support the NRC's longer term goals related to the improvement of URANS based turbulence models in stratified layer erosion processes. This is an area where common isotropic turbulence models used in CFD codes have difficulty predicting the mixing behavior. The NRC has worked with its OECD/NEA HYMERES-2 partners to get the testing approved and completed.

The ultimate goal of this work is to improve faster-turn-around lower-fidelity modeling of (anisotropic) turbulence- and buoyancy-driven mixing that are typically based on isotropic turbulence modeling closures. Here we describe next steps toward this goal after last year's initial scoping simulations.

2.1 Previous Year Solution Analysis

Last year's meshing, testing, and simulation campaign highlighted the importance of determining appropriate geometry simplification and efficient boundary condition (BC) modeling. In particular, will the BC of fully developed turbulent pipe flow in a shorter inlet (e.g., using a recycling technique) suffice (e.g., [7]) or more HYMERES-2's upstream geometry complexity is necessary to include with,

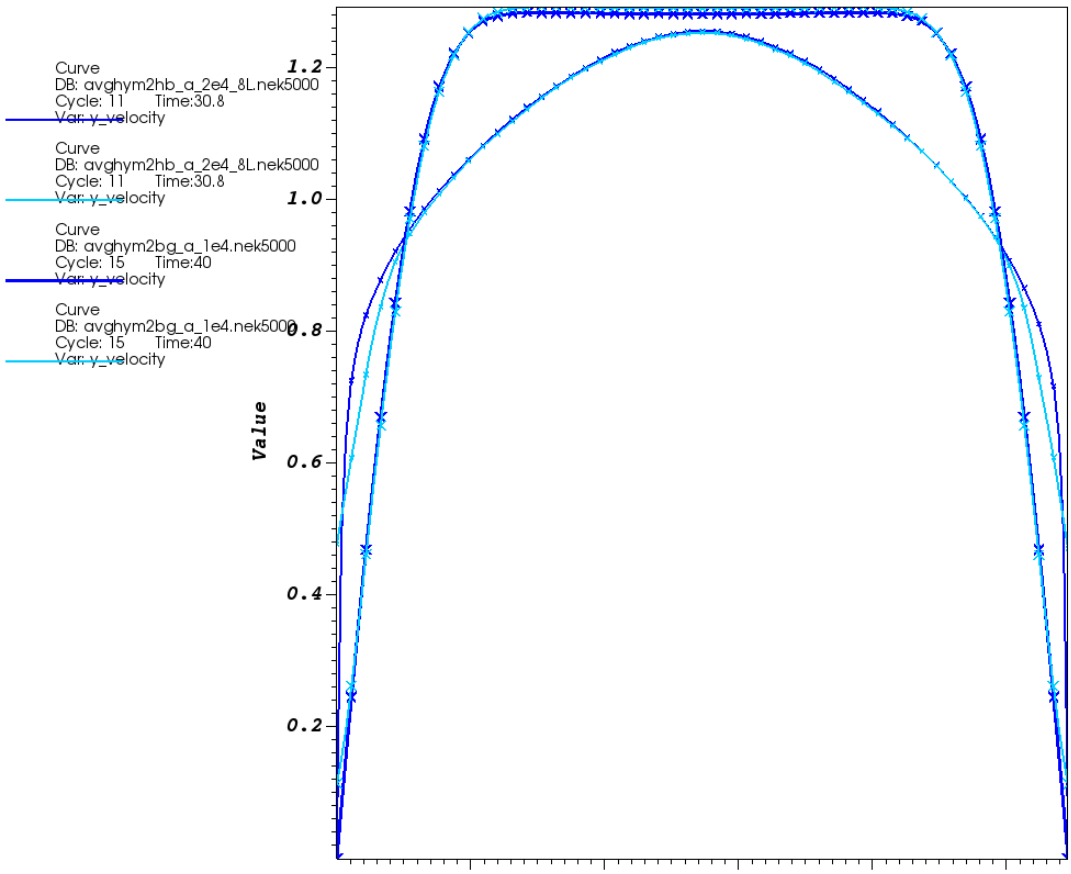

Figure 1: Mean vertical velocity in hydro LES of HYMERES-2 geometry with "uniform" inlet for Re=10^4 (small crosses) and 2×10^4 (large crosses) at two pipe inlet heights.

perhaps, synthetic eddy/turbulence modeling?

Figure 1 justifies the effort highlighting the importance of BC modeling where comparison of mean vertical velocity profiles in last year's hydro LES of HYMERES-2 geometry with "uniform" inlet is plotted for two Reynolds numbers/flow rates at two axial locations. Note that since we have reached only verbal agreement with PSI to release the benchmark specification and make the test open, we are still plotting this result and all other figures without full details that will be provided once the NDA is finally lifted.

This comparison illustrates that flow with a uniform inlet BC is still developing and since the target Reynolds number Re for final benchmark runs is in between the values in Figure 1, a careful study of the sensitivity of the pipe inlet LES to its geometry and upstream level of turbulence is in order for the HYMERES-2 specification regime.

2.2 Inlet Sensitivity Study

Despite having ("curved") axial symmetry, the HYMERES-2 inlet has a rather complicated shape consisting of multiple bends and changes of the pipe diameter. Due to the large disparity of spatiotemporal scales in the benchmark flow, every bit of simplification is important, including a possible simplification in the inlet geometry and its' turbulence level modeling. Naturally, the first question that must be addressed is whether more simple modeling, i.e. a fully-developed pipe profile, is a good enough approximation or if more of the upstream geometry and/or the inlet synthetic turbulence modeling is necessary. Preliminary experimental results were not conclusive enough so we have embarked on a series of inlet geometry complication setups ranging from the simplest fully-developed flow pipe (with periodic conditions) to multiple upstream bends and diameter changes. Moreover, we also wanted to provide data for cross-verification comparison against solutions with tools that NRC staff are currently employing for these types of problems, such as using URANS modeling available in commercial CFD packages.

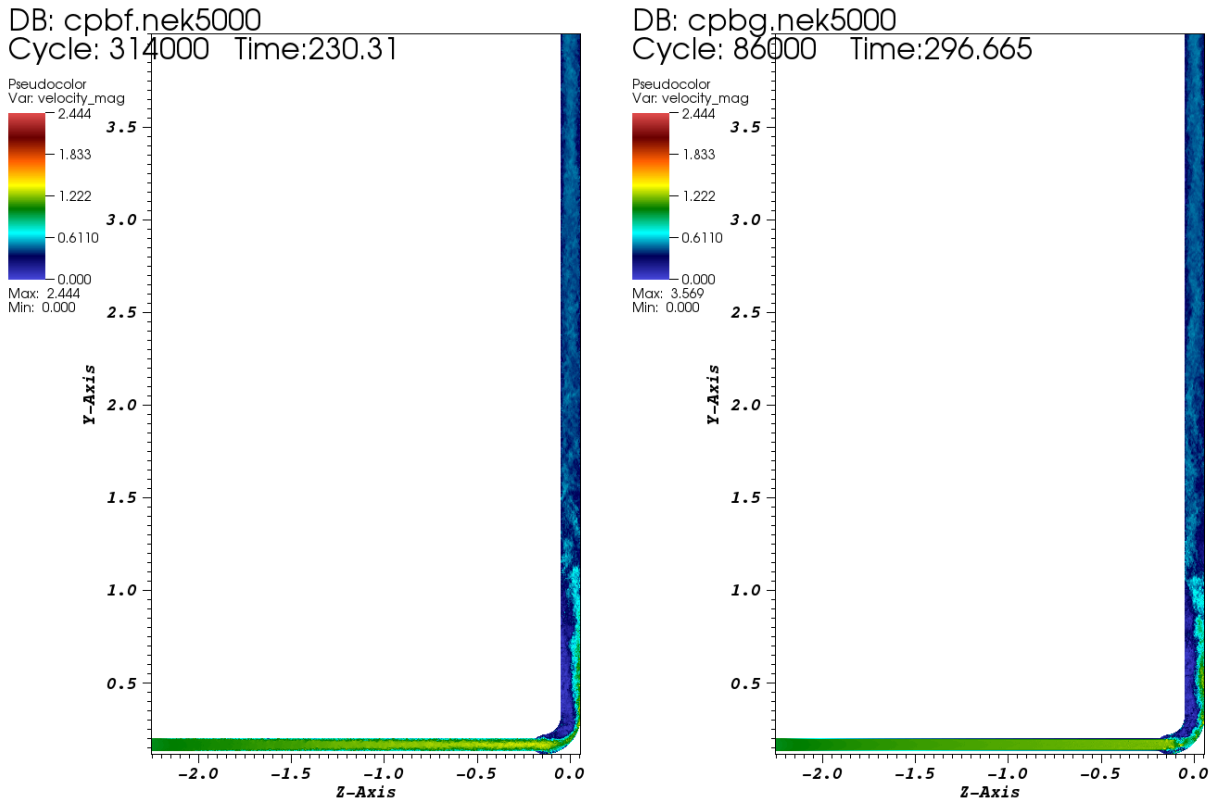

(a) $N = 4$ (b) $N = 6$

Figure 2: Instantaneous magnitudes of velocity in a single-bend configuration with increase of resolution at $x = 0$.

Figure 2 shows velocity magnitude in LES of a single bend configuration of HYMERES-2 inlet with increase of resolution by means of polynomial degree N of the Gauss-Lobatto-Legendre quadrature points per each orthogonal direction of a (canonical) spectral element. Note that both

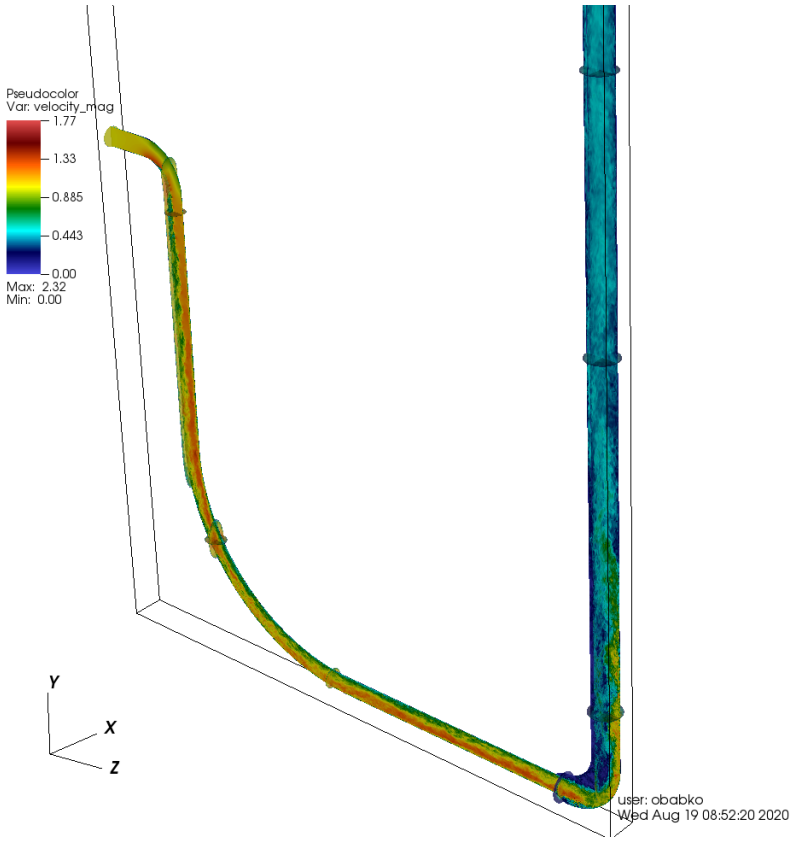

Figure 3: Instantaneous magnitudes of velocity in a triple-bend configuration with an increase of resolution at $x = 0$.

solutions have the same uniform flow BC. Despite the spectral convergence with increase of N, the solution near the bend seemed to be too sensitive to resolution.

To resolve this apparent paradox, it was hypothisized that due to linearly stable nature of the pipe flow, higher numerical resolution in $N = 7$ case (Figure 2b) leads to more (numerically-produced) noise that is further (algebraically) amplified into more/stronger (coherent) vortical structures resulting in transition to turbulence inside the horizontal branch of this variant of HYMERES-2 inlet test configuration. Therefore, to test the consistency of this explanation, the flow simulation at the same $N = 7$ (and thus same amount of subgrid/numerical dissipation due to Nek-standard spectral damping/explicit filtering) but with the fully-developed turbulent inlet should sustain turbulence production all the way into the bend which was later fully confirmed (cf. Figure 5).

In any case, it was still important to look into another, more complex, HYMERES-2 inlet configuration that bears closer resemblance to the actual benchmark flow upstream. Figure 3 shows instantaneous velocity magnitude of LES in a triple bend case plotted on representative cross-sections including the cut at $x = 0$ used in Figure 2. This configuration solution starts with uniform inlet flow and quickly becomes turbulent after the additional bend being fully turbulent upstream of the last downstream bend used in cases of Figure 2.

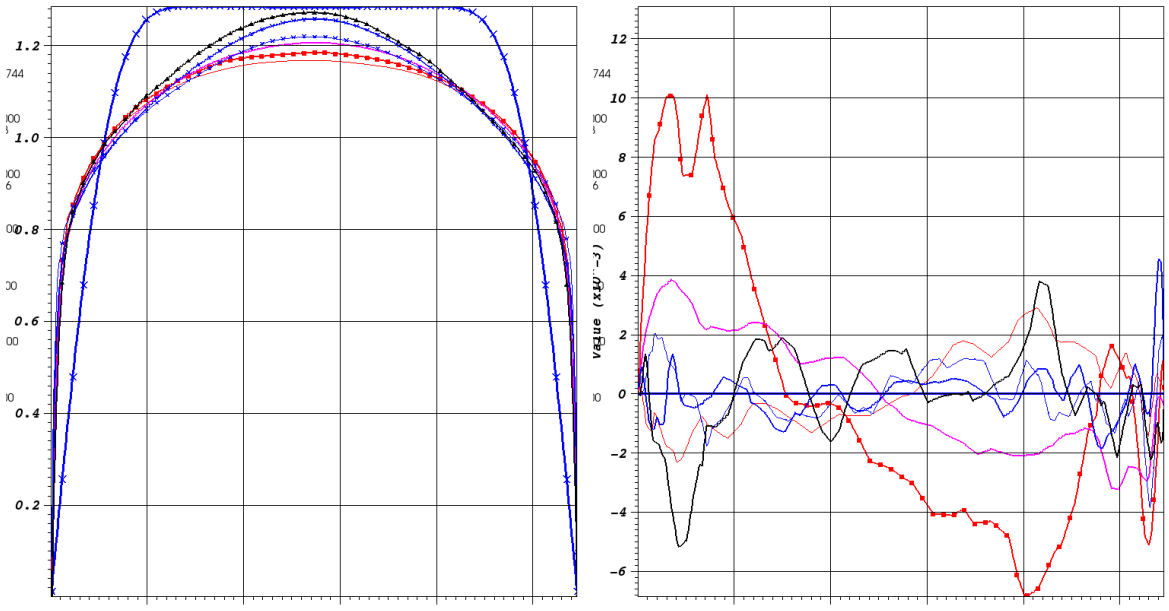

(a) axial (b) horizontal

Figure 4: Mean velocity component profile across the outlet.

Figure 4 summarizes most of the findings of the sensitivity study so far. The axial velocity (Figure 4a) in bend cases, single with $N = 4$ (red line) and $N = 7$ (pink line) and triple (red squares), are similar in shape and close to both the high-Re HYMERES-2 low-res (thin blue line with crosses) and high-res (thick blue line with crosses) cases being drastically different from the developing case of low-Re HYMERES-2 run (blue line with large crosses – cf. Figure 1). Apart from the latter case, all other variations of inlet conditions do not differ from the periodic/fully-developed turbulent case (black line) by more than approximately 8% which was found to be within the estimated experimental mass flow uncertainty provided by the NRC staff. Figure 4b establishes that the horizontal velocity is within the numerical convergence/averaging noise thus excluding non-negligible swirl flow influence on the outlet cross-section field downstream of the bends. Thus the fully-developed flow entering into the PANDA vessel seems to be a good approximation to the HYMERES-2 tests, with a recycling inlet, that avoids more costly/rather ambiguous synthetic eddy/turbulence methods.

Finally, we have checked for sustainability of turbulence at the same conditions as in Figure 2b but with a turbulent/recycling flow inlet. As hypothesized earlier, the introduction of the turbulent/coherent structures at a sufficient level makes all the difference for flow transition to turbulence upstream of the last downstream bend as shown in Figure 5.

In summary, this study has confirmed that modeling the HYMERES-2 inlet as a short pipe with fully-developed turbulent flow using a recycling technique is adequate enough for modeling the PANDA vessel entrance flow.

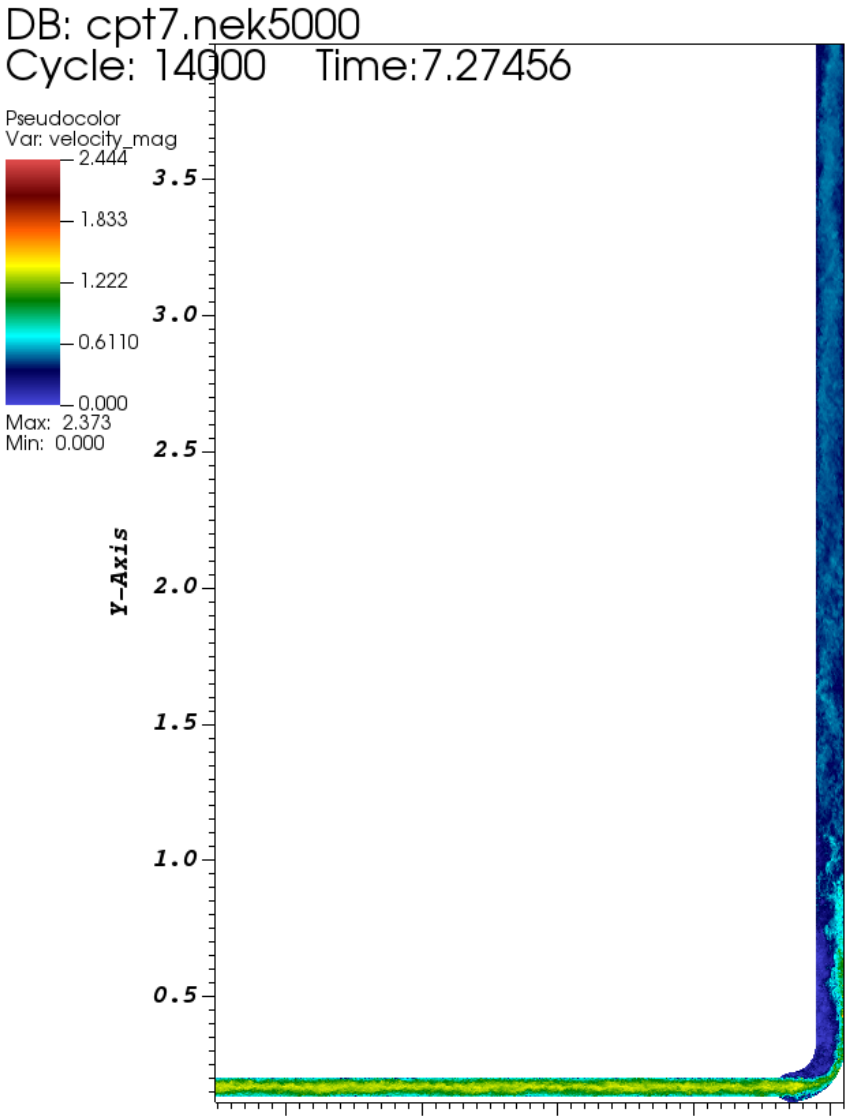

Figure 5: Instantaneous magnitudes of velocity in a single bend configuration with turbulent inlet/recycling BC at $x = 0$.

2.3 HYMERES-2 Turbulent Inlet Setup

After careful sensitivity studies of LES in pipe inlet geometry and conditions of the benchmark in Section 2.2, we have implemented and tested the LES solutions on a new mesh. This mesh has a smaller element count (and slightly different/more efficient element layout) that takes advantage of last year's effort (Section 2.1) and earlier study (Section 2.2) that settled the inlet flow modeling for the recycling/fully-developed flow. As a first step, we focus on the HYMERES-2 configuration without an obstacle.

Figure 6 illustrates the hydro flow evolution for the final specification of cross-verification campaign that also will be used for further heat and mass transfer runs with buoyancy effects. To highlight the three-dimensional aspect of the flow, the latter figure (Figure 6b) is plotted in 3D in Figure 7.

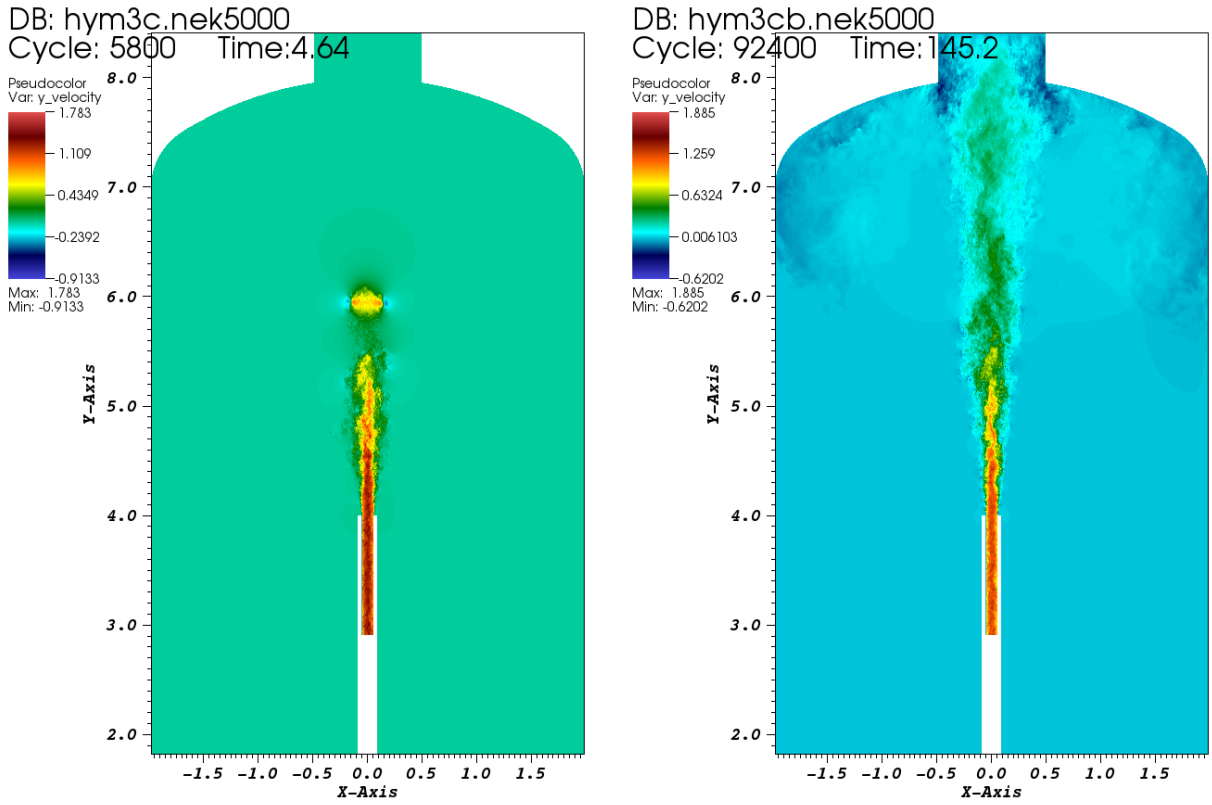

(a) close to startup (b) later in time

Figure 6: Instantaneous vertical velocity in the cross-verification HYMERES-2 setup at $x = 0$.

Preliminary comparison by NRC staff shows that Nek5000 fully developed inlet results are in the ballpark of the PSI data after accounting for the mass flow rate uncertainty estimate.

The next steps are to finish testing the setup of the heat and mass transfer case with buoyancy and to validate the results with PSI data.

2.4 INL HPC Support and Miscellaneous

In addition to last year's effort when the U.S. NRC staff started using HPC resources of the ALCF during the (last IBM BG/Q's) INCITE allocation, we have continued providing support for other HPC resources.

First, we have written a successful ALCC proposal for the ALCF Theta resource as a follow-up to INCITE, where some of the calculations in Section 2.2–2.3 were conducted. Moreover, we assisted

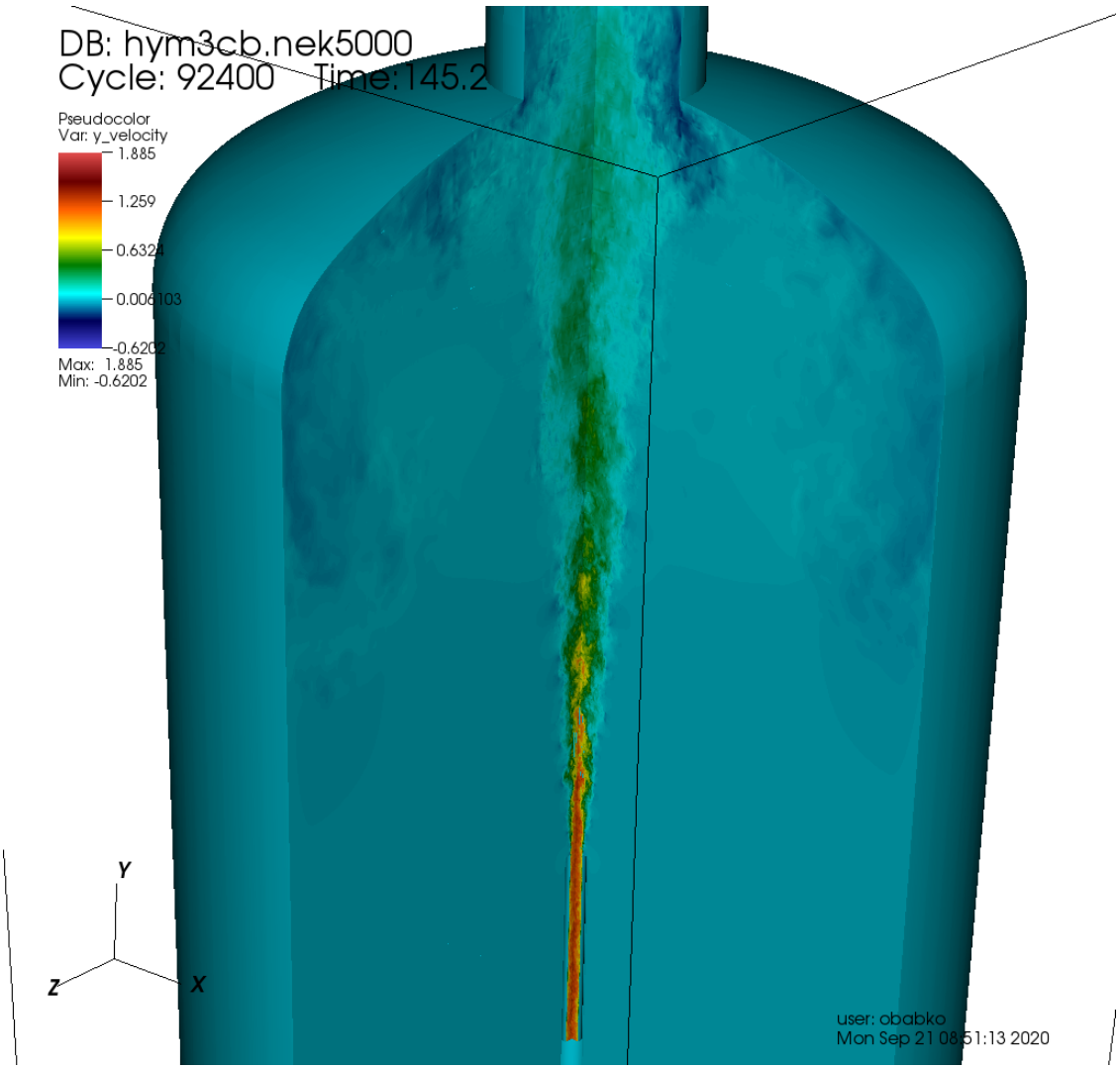

Figure 7: Instantaneous vertical velocity in the cross-verification HYMERES-2 setup .

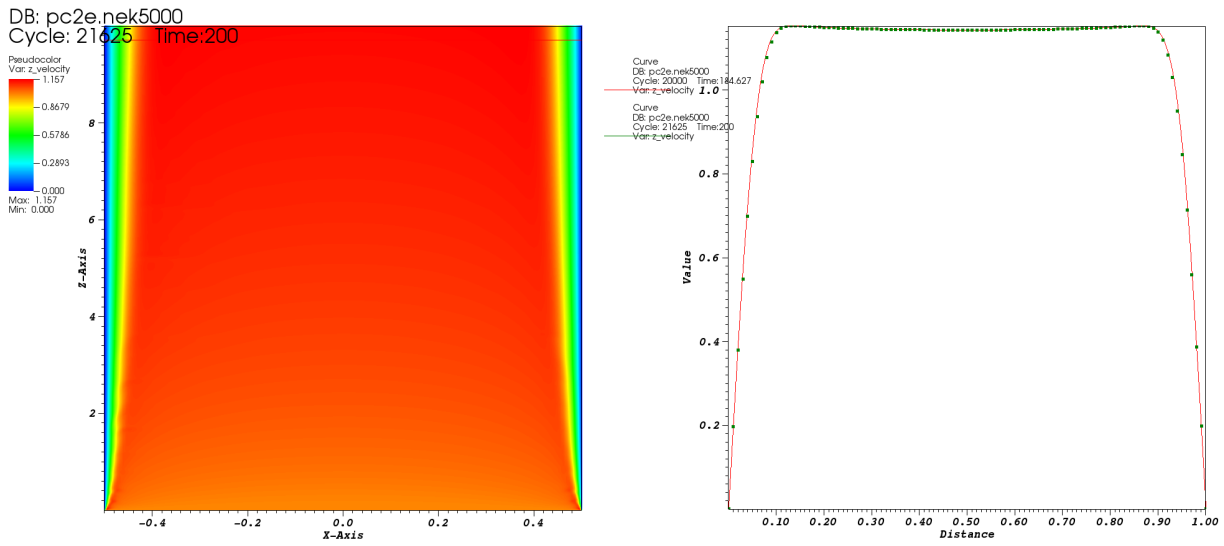

(a) axial velocity (b) its axial profiles

Figure 8: Instantaneous vertical velocity in the NRC pipe test setup.

NRC staff with compilation and job submission on the INL HPC clusters Falcon and Sawtooth. The latter platform has been used for the Nek5000 pipe test case that is fully meshed, modified, and coded by the NRC staff with only minor consultancy of the ANL team.

Figure 8 shows axial velocity and its axial profiles close to the outlet at two time instances for the uniform inlet BC illustrating the steady-state convergence of this pipe test case set up by NRC staff. This first test case is a laminar developing flow to check mesh and BC prescription. The goal is to set up and conduct LES of this canonical geometry.

Thus, the next round of runs for this mesh is a turbulent fully developed flow simulation using a recycling technique with assistance from the ANL team. Figure 9 shows typical fully developed turbulent instantaneous velocity components. The only unusual feature of this canonical case is that the first attempt of its meshing resulted in a rather fine element mesh count for the chosen Reynolds number so it was possible to get a decent LES using $N = 2$; therefore, for the typical values of polynomial degrees used in Nek5000 (e.g., $N = 8$), we can run this case at a higher Re and/or fidelity if needed.

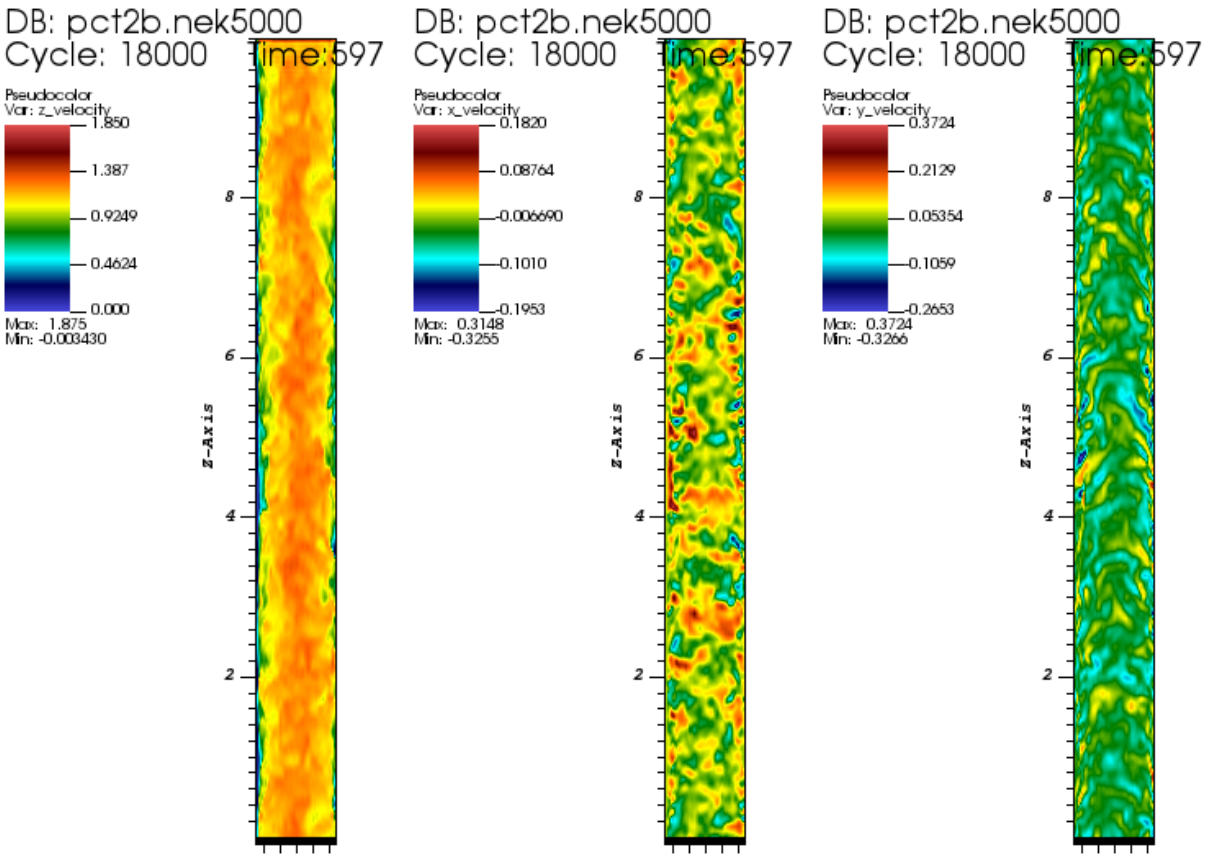

(a) axial (b) wall normal (c) binormal

Figure 9: Instantaneous velocity components in the LES of NRC turbulent pipe test case.

3 Reynolds-Averaged Navier-Stokes Solvers

Several of the applications of interest to NEAMS can be addressed through RANS modeling of turbulence. The RANS models implemented in Nek5000 are based on the $k-\omega$ model, which includes the turbulent kinetic k enegy and the specific dissipation rate ω (or its inverse τ) in addition to the velocity field $\mathbf{v}$. The model describes the turbulent properties of incompressible flows with

$$k = \frac{\langle u'^2 \rangle + \langle v'^2 \rangle + \langle w'^2 \rangle}{2}, \tag{1}$$

where u', v', and w' are the fluctuation components of the velocity vector around the ensemble-averaged mean velocity vector $\mathbf{v} = (u, v, w)$ governed by

$$\frac{\partial(\rho\mathbf{v})}{\partial t} + \nabla\cdot(\rho\mathbf{v}\mathbf{v}) = -\nabla p + \nabla\cdot\left[(\mu+\mu_t)\left(2\mathbf{S} - \frac{2}{3}Q\mathbf{I}\right)\right], \tag{2}$$

$$\frac{\partial(\rho k)}{\partial t} + \nabla\cdot(\rho k\mathbf{v}) = \nabla\cdot\left[(\mu+\frac{\mu_t}{\sigma_k})\nabla k\right] + P - \rho\beta^* k\omega, \tag{3}$$

$$\frac{\partial(\rho\omega)}{\partial t} + \nabla\cdot(\rho\omega\mathbf{v}) = \nabla\cdot\left[(\mu+\frac{\mu_t}{\sigma_\omega})\nabla\omega)\right] + \gamma\frac{\omega}{k}P - \rho\beta\omega^2 + S_\omega, \tag{4}$$

where

$$\mathbf{S} = \frac{\mathbf{1}}{\mathbf{2}}\left(\nabla\mathbf{v} + \nabla\mathbf{v}^{\mathbf{T}}\right),$$

μ is the molecular viscosity and μ_t is the turbulent viscosity, with the continuity equation for incompressible flow being

$$Q = \nabla\cdot\mathbf{v} = 0. \tag{5}$$

The divergence of velocity Q can be nonzero in the case of reactive or multiphase flows. The term S_ω corresponds to cross-diffusion and is nonzero only for the kw06 model. (We denote the Wilcox 1998 [8] and 2006 [9] versions as kw98 and kw06, respectively.)

We have implemented and tested several RANS approaches in Nek5000, in the frame of the spectral element method (SEM), including a regularized version of the $k-\omega$ model [10, 11, 4]. A significant development during the past year was the implementation and testing of the $k-\tau$ model, which was originally developed by Kalitzin et al. [5, 6] as an alternative implementation of the standard $k-\omega$ model.

In contrast to the original form of the $k-\omega$ model, in which the ω equation contains terms that become singular close to wall boundaries, all terms in the right-hand side of the k and τ equations reach a finite limit at walls and do not need to be treated asymptotically; that is, they do not require regularization for numerical implementation. Moreover, this model does not rely on the wall-distance function or its derivatives.

The equations for k and τ are derived from the $k-\omega$ equations by using the definition $\tau = 1/\omega$:

$$\frac{\partial(\rho k)}{\partial t} + \nabla \cdot (\rho k \mathbf{v}) = \nabla \cdot \left[(\mu + \frac{\mu_t}{\sigma_k}) \nabla k \right] + P - \rho \beta^* \frac{k}{\tau}, \tag{6}$$

$$\frac{\partial(\rho \tau)}{\partial t} + \nabla \cdot (\rho \tau \mathbf{v}) = \nabla \cdot \left[(\mu + \frac{\mu_t}{\sigma_\omega}) \nabla \tau \right] - \gamma \frac{\tau}{k} P + \rho \beta - 2 \frac{\mu}{\tau} (\nabla \tau \cdot \nabla \tau), \tag{7}$$

where P is the rate of production of TKE. The last term in the τ equation was implemented in the form proposed by [12], as

$$S_\tau = 2\nu (\nabla \tau \cdot \nabla \tau) / \tau = 8\nu \left(\nabla \tau^{1/2} \cdot \nabla \tau^{1/2} \right). \tag{8}$$

Looking closer into the scaling of all the terms appearing in the right-hand side of the k and τ equations, one can observe that near walls, the two main terms of the k equation balance each other:

$$Y_k = \rho \beta^* \frac{k}{\tau} \approx \mu \nabla^2 k,$$

whereas the dissipation and diffusion terms in the τ equation behave as

$$Y_\tau = \rho \beta \rightarrow \rho \beta$$
$$\nabla \cdot (\mu \nabla \tau) \rightarrow \frac{1}{3} \rho \beta$$
$$S_\tau = 2 \frac{\mu}{\tau} (\nabla \tau \cdot \nabla \tau) \rightarrow \frac{4}{3} \rho \beta.$$

As described in the next subsections, we also investigated ways to increase the stability, accuracy, and robustness of our RANS approaches in order to be able to use larger timesteps. In a separate, ongoing effort described below we are extending these models to support steady-state solvers. The objective here is to accelerate convergence for turbulent flows in complex geometries. We will continue to develop these solvers to make them effective for production-level simulations at scale.

3.1 Implicit Treatment of Source Terms in the Model Equations

To increase the timestep in unsteady RANS simulations, we have treated several of the terms appearing in the right-hand side of the model equations implicitly for stabilization, as explained below by including them in the left-hand side of the implicit/explicit solution procedure. The terms that were treated implicitly are the following: For the $k - \omega$ model these are (i) the dissipation term in the k equation (Y_k) and (ii) two terms in the right-hand side of the ω equation that become unbounded close to walls at the same rate and need to be grouped together. For the $k - \tau$ model these terms are (i) the dissipation term in the k equation (Y_k) and (ii) the last term S_τ in the τ equation, which can become a source of instability as well as the cross-diffusion term of the kw06

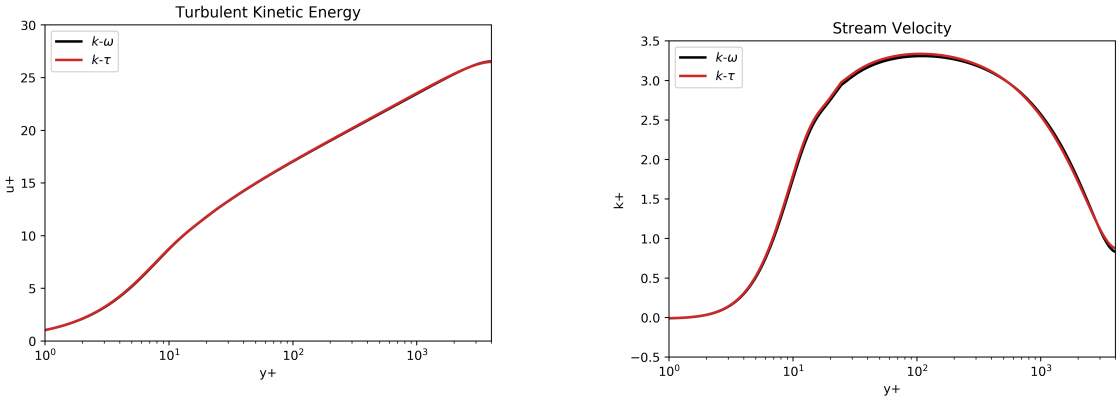

Figure 10: Comparison of mean streamwise velocity u^+ and turbulent kinetic energy k^+ profiles for $k-\omega$ and $k-\tau$ models.

model, S_ω.

With the implicit treatment of these terms the timestep is restricted by the convective CFL number, which for the BDF scheme is approximately 0.5 whereas for the OIFS (characteristics) convective scheme it can reach the value of 4. This timestep increase has been achieved without increasing the computational cost. A publication on this topic is currently in preparation, and we plan to continue the investigation of this model further for the study of complex flows.

3.2 Verification and Validation of RANS Models in Nek

Extensive verification and validation tests of the models were performed for turbulent channel flow and flow past a backward-facing step (BFS), as well as external flows such as flow past a wind turbine blade and the NACA0012 airfoil at angle of attack aoa=0 and 10.

Figure 10 shows the comparison of results from the regularized $k-\omega$ and the $k-\tau$ model for flow in a channel at $Re = 10,950$. As can be observed, the two models give almost identical results for the mean velocity and the turbulent kinetic energy as well as all for other variables.

The flow past a BFS at $Re = 149,700$ (Driver et al. [13]) was simulated by using the $k-\tau$ model, and results were compared with the results of the regularized $k-\omega$ model (published in [4]). Figure 11 shows isocontours of the mean streamwise velocity u and the k at steady state. The length of the recirculation zone from the RANS simulation using the $k-\tau$ model with the kw98 coefficients is equal to $6.59H$ (where H is the step height) and was found to be in excellent agreement with the corresponding value obtained by using the regularized $k-\omega$ model ($6.58H$). The recirculation zone length for the kw06 version is equal to $6.53H$.

We also investigated the performance of the $k-\tau$ model and compared it with the regularized $k-\omega$ model results (described in the preceding subsection) for the benchmark case of flow past

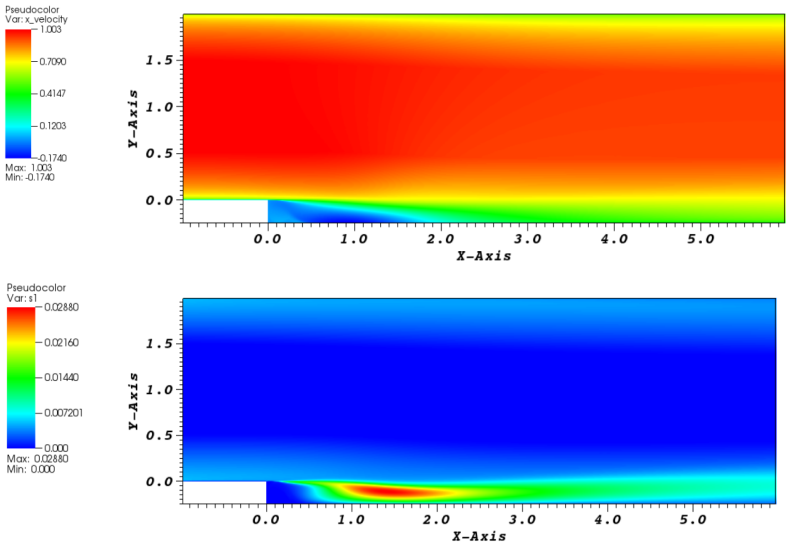

Figure 11: Comparison of mean streamwise velocity u^+ and turbulent kinetic energy k^+ profiles for the BFS at $Re = 149,700$ using the $k-\tau$ model of kw98.

the NACA0012 airfoil at aoa=0 and 10, which is relevant for external flows. The values of the drag and lift coefficients obtained with the $k-\tau$ model are also shown in Tables 1 and 2 for the two versions of the model using varying resolution at $Re = 6 \times 10^6$. As can be observed in these tables, the drag and lift coefficients are in very good agreement both with the regularized $k-\omega$ model results and with the benchmark values from the NASA LARC website. In addition, as can be observed, as resolution improves by increasing the polynomial order from $N = 7$ to $N = 11$ (8 and 12 points per direction, respectively), the models converge to the benchmark values of the drag and lift coefficients, which are also shown in the tables. Figure 12 shows the isocontours of the mean streamwise velocity u^+ and turbulent kinetic energy k^+ profiles at steady state for the case of $Re = 6 \times 10^6$ and aoa=10 and computed by using the $k-\tau$ model of kw98.

We investigated the performance of several limiters, commonly used in the RANS literature, for the production terms in the k and ω equations as well as for the eddy viscosity.

We found that for external flows it is important to limit the value of eddy viscosity in the far field, which is typically not well resolved, in order to avoid abrupt variations in total viscosity. Such variations can cause stability problems to the simulation and/or can significantly increase the number of pressure/velocity iterations needed for convergence at every timestep. The performance of the modified version of the $k-\omega$ model was tested for flow past a NACA0012 airfoil geometry, with varying free-stream conditions. With the modifications described above we obtained fully converted results for the drag and lift coefficients even for zero free-stream values of k.

For external flows, the $k-\tau$ model can also exhibit similar undesirable far- field artefacts. The τ field can continue to grow outside boundary layers and can reach maximum values well away from surfaces of interest (e.g., airfoils), where k is negligible. In this way high levels of τ can be present

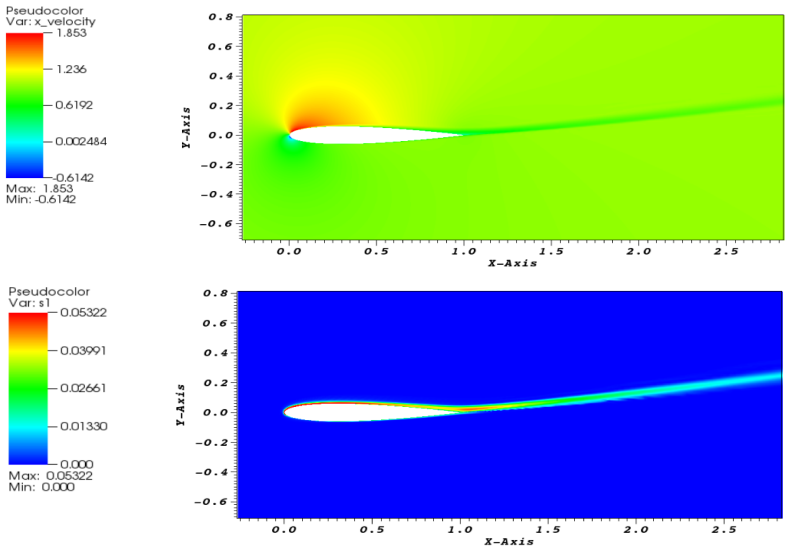

Figure 12: Comparison of mean streamwise velocity u^+ and turbulent kinetic energy k^+ profiles for the flow past a NACA0012 airfoil at $Re = 6M$ and a 10° angle of attack using the $k-\tau$ model of kw98.

in the freestream, and because of the convective and diffusive terms these high levels of τ can be maintained further downstream. This is an undesirable effect; and in order to suppress it, a limiter as described in [5] has been implemeted and tested. For the $k-\tau$ model, the equation for μ_t is $\mu_t = \rho k\tau$ and the limiter is defined as

$$R = \max\left(0.01\mu, \rho k\tau\right).$$

The production P, dissipation Y_τ and S_τ, source terms in the τ equation are multiplied by the ratio μ_t/R; and the limiter, R, is chosen such that in regions of the flow where the eddy viscosity is larger than 1% of the laminar viscosity, the source terms are unaffected. In this way the far field remains completely free from any artefacts in the τ solution.

Table 1: Drag and lift coefficients (aoa=0). Experimental data: NASA-TM-4074 [14].

	Nek5000 results				References		Exper.
model	kw98 (N=7/N=11)	kτ98 (N=7)	kw06 (N=7/N=11)	kτ06 (N=7)	CFL3D	FUN3D	
drag	0.00872 / 0.00843	0.00842	0.00861/0.00833	0.00832	0.00854	0.00837	∼0.0081
lift	±1E-5/±1E-5	1.55E-5	±1E-5/±1E-5	1.21E-5	∼0	∼0	∼-0.01

Overall, we have found that the $k-\tau$ model gives exactly the same results with the $k-\omega$, and for this reason we investigated this model more extensively and plan to use it further to study more complex flows.

Table 2: Drag and lift coefficients (aoa=10). Experimental data: NASA-TM-4074 [14].

	Nek5000 results				References		Exper.
model	kw98 (N=7)	kτ98 (N=7)	kw06 (N=11)	kτ06 (N=7/N=9)	CFL3D	FUN3D	
drag	-	0.01507	0.01391	0.01468/0.01432	0.01259	0.01297	$\sim$ 0.012
lift	-	1.0582	1.0639	1.0592/1.0609	1.0958	1.1012	$\sim$ 1.075

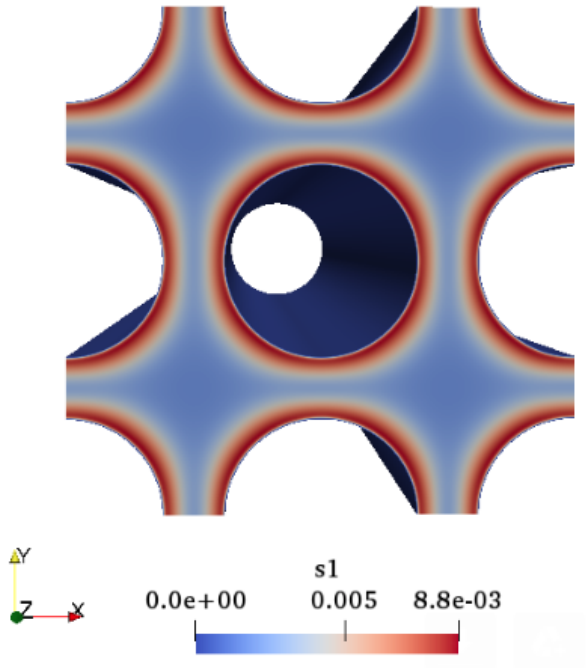

Figure 13: Distribution of TKE along the outflow plane.

3.3 Implementation of RANS Models in nekRS

Because of its demonstrated robustness and stability as discussed above, the $k-\tau$ model is the only RANS model that has been implemented in the new GPU version of the Nek5000 code, called nekRS. Preliminary tests using both codes have demonstrated that the model implemented in nekRS gives results identical to the results with Nek5000 for several benchmark problems. A case involving a more complex geometry is shown in Figures 13 wnd 14 for a 2x2 subchannel rod bundle, in which nekRS is able to reproduce the same solution as Nek5000 to high accuracy in terms of k and tau distributions along the domain outlet and specifically along the subchannel diagonal line.

3.4 Buoyancy Models

In order to account for the effects of buoyancy, a two-dimensional differently heated square cavity was considered as a test case to evaluate modifications to the $k-\tau$ turbulence model implemented

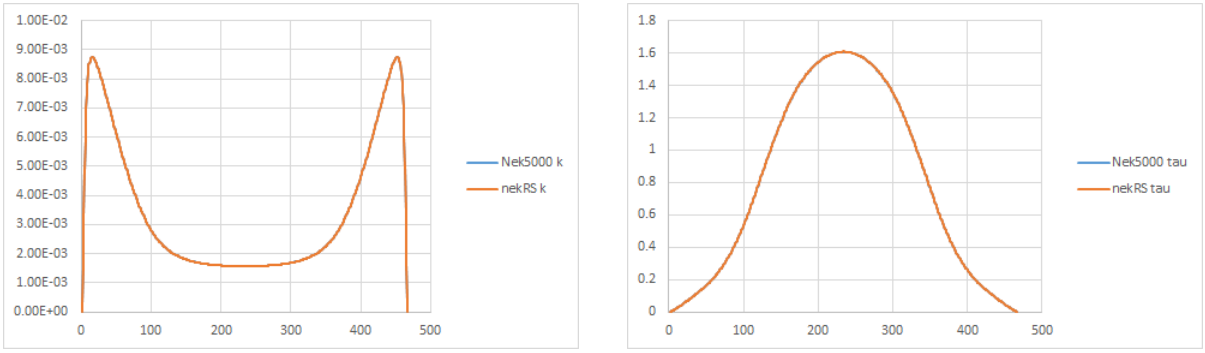

Figure 14: Comparison of turbulent kinetic energy k and τ profiles along the subchannel diagonal line for the flow in a 2x2 rod-bundle case between Nek5000 and nekRS.

in Nek5000. The standard $k-\tau$ model, first presented in [5], is used in the present work because of its simplicity since it does not strictly require a wall-damping function and because singular behaviors at solid walls are avoided. Two models for the turbulent heat flux are considered in the present work: the Simple Gradient Diffusion Hypothesis (SGDH) and the General Gradient Diffusion Hypothesis (GGDH), which are described in [15]. The cavity considered is identical to the problem in [16], where the authors performed a real experiment and collected data to serve as a benchmark. In this work the experiment carried out gives a Rayleigh number of $1.58(10^9)$. We note that the differently heated square cavity is known to be a simple problem in heat transfer and hence might not be the most suitable case to evaluate buoyancy modeling. Indeed, other cases would be more suitable to evaluate such modeling, for example, concentric and eccentric horizontal annuli problems [17]. However, a simple cavity problem category problem is a convenient way of testing the iimplementation of neww models in Nek5000, which is the main objective of the present work.

Model Formulation

The standard $k-\tau$ model as previously described has been modified to account for production of k and τ due to buoyancy. Specifically, terms must be added to Eqs. (6 and 7) to account for buoyancy:

$$\frac{\partial(\rho k)}{\partial t}+\nabla\cdot(\rho k\mathbf{v}) = \nabla\cdot\left[(\mu+\frac{\mu_t}{\sigma_k})\nabla k\right]+P-\rho\beta^*\frac{k}{\tau}+B_k, \tag{9}$$

$$\frac{\partial(\rho \tau)}{\partial t}+\nabla\cdot(\rho \tau\mathbf{v}) = \nabla\cdot\left[(\mu+\frac{\mu_t}{\sigma_\omega})\nabla \tau\right]-\gamma\frac{\tau}{k}P+\rho\beta-2\frac{\mu}{\tau}\left(\nabla\tau\cdot\nabla\tau\right)+B_\tau. \tag{10}$$

Where B_k and B_τ are the extra production terms due to buoyancy:

$$B_k = g_i\beta\overline{u_j'T'}, \tag{11}$$

$$B_\tau = \frac{\alpha_\omega\tau}{k}B_k, \tag{12}$$

In a RANS framework, the turbulent heat flux, $\overline{u'T'}$, is not directly available and must be modeled. Two hypotheses are commonly adopted [15]: the Simple Gradient Diffusion Hypothesis (SGDH) and the General Gradient Diffusion Hypothesis (GGDH). For the SGDH, the turbulent heat flux is modeled as

$$\overline{u_j'T'} = -\frac{\nu_t}{Pr_t}\frac{\partial T}{\partial x_j} \tag{13}$$

and for the GGDH

$$\overline{u_j'T'} = -C_s\overline{u_j'u_k'}\frac{k}{\varepsilon}\frac{\partial T}{\partial x_j}. \tag{14}$$

Problem Formulation

Simulations of a differently heated cavity are performed at $Ra = 1.58(10^9)$. This is based on the temperature difference between the vertical walls, the cavity size L, and the fluid properties

$$Ra = \frac{g\beta L^3(T_h - T_c)}{\nu\alpha}, \tag{15}$$

where T_h is the hot wall temperature, T_c is the cold wall temperature, β is the thermal expansion coefficient, ν is the kinematic viscosity, and α is the thermal diffusivity.

In this model a constant fluid density was used with the Boussinesq approximation to account for buoyancy. This was done by adding a body force of the form

$$f_i = g_i\beta(T - T_{ref}), \tag{16}$$

where the reference temperature was chosen as the arithmetic mean between the hot and cold walls. The mesh employed 40×40 elements over the cavity and used a polynomial approximation order of 8. The mesh was designed to ensure $y^+ < 1$ near the wall. A de-aliasing procedure based on the 2/3 rule was also employed.

Results

In this section esults are presented and compared against benchmarked data from [16] along the half-height of the cavity, namely, $y/L = 0.5$, for all cases considered here. Figures 15–17 show the profiles of the vertical velocity, the turbulent kinetic energy, and the temperature, respectively. Note that the buoyancy velocity, $V_0 = \sqrt{g\beta L(T_h - T_c)}$, is used here as a normalization parameter.

From these results we can see that the two variants implemented for the buoyancy, namely, SGDH and the GGDH, provided better behavior for the variables investigated when compared with the unmodified $k - \tau$ model. Moreover, Table 3 provides the standard deviation of the discrepancy between the variables of each model considered for the experimental data. This parameter is taken to be an uncertainty measure of how agreed is each model to the benchmarked data. These values allow us to conclude that from the statistical point of view, both models were able to improve the turbulence model when accounting for buoyancy effects. However, we notice that the difference in

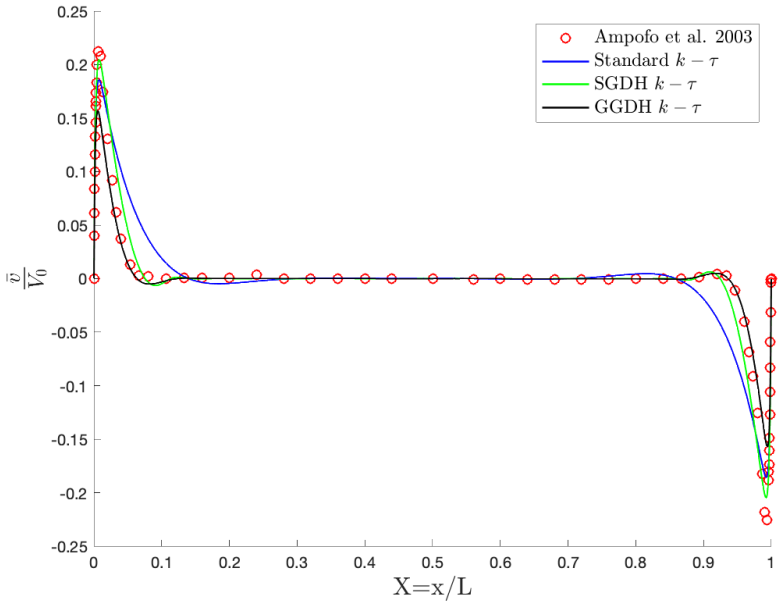

Figure 15: Vertical velocity profiles at $y/L = 0.5$.

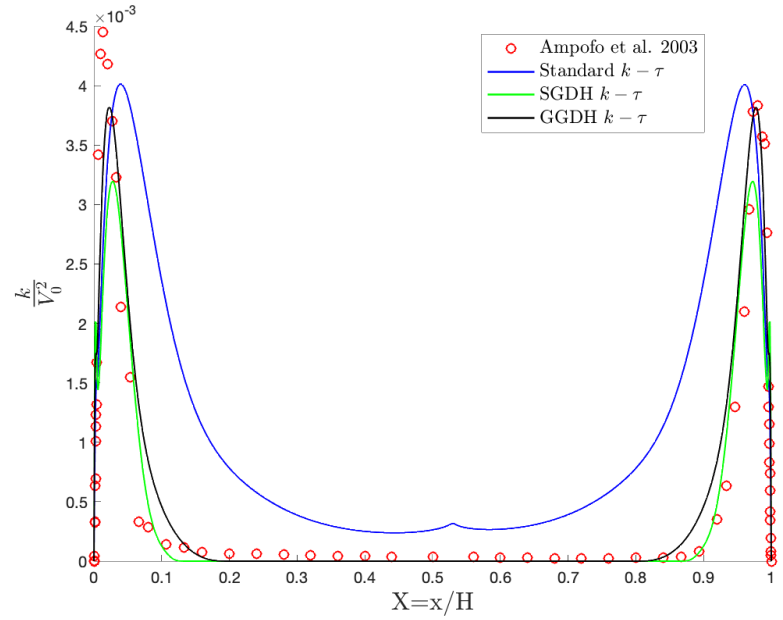

Figure 16: Turbulent kinetic energy ($k \equiv \frac{1}{2}\overline{u'u'}$) profiles at $y/L = 0.5$.

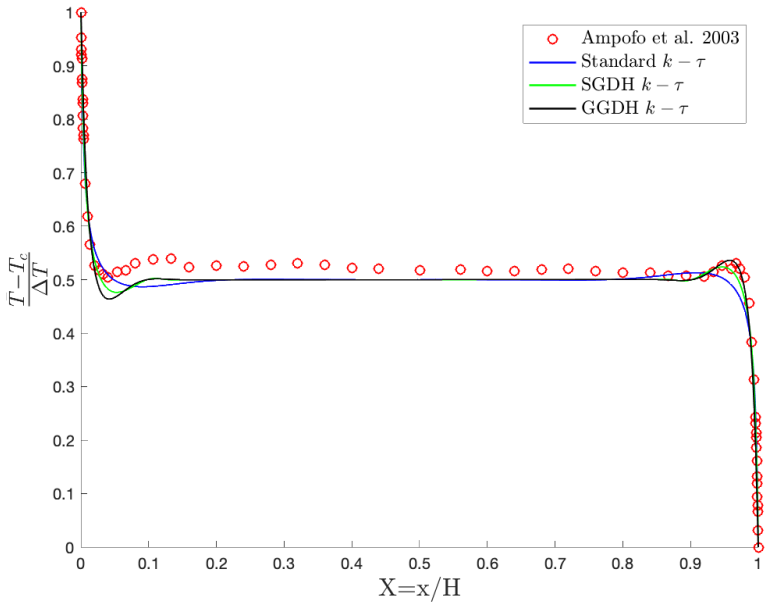

Figure 17: Temperature profiles at $y/L = 0.5$.

the peak, specifically for the vertical velocity, is in better agreement with the experimental data when using the SGDH rather than using the GGDH. A reasonable explanation for this difference is that the flow in the case studied is known to be stratified because of to the simplicity of the case and, as will be discussed, the GGDH is better suited for flows with high anisotropy, for example, forced convection. On the other hand, the SGDH relies on the assumption that the turbulent heat flux is essentially isotropic, which may be the reason that this model yields much better results, in particular for the differently heated square cavity.

Table 3: One standard deviation of the differences between solution variables and the experimental data for the unmodified $k-\tau$, the SGDH, and GGDH models

	$\frac{v}{V_0}$	$\frac{k}{V_0^2}$	$\frac{T-T_c}{T_h-T_c}$
$\sigma_{k-\tau}$	0.0201	$8.6549(10^{-4})$	0.0146
σ_{SGDH}	0.0099	$3.5013(10^{-4})$	0.0106
σ_{GGDH}	0.0102	$2.8093(10^{-4})$	0.0126

The SGDH relies on the assumption that the turbulent heat component is aligned to the temperature gradient; see Eq. (refeq:sgdh). This assumption makes the SGDH model fairly straightforward to implement compared with the GGDH, since it relies on a scalar value for the diffusion coefficient. Nek5000 allows for this to be included as a variable coefficient in the Helmholtz solve, as is typically done with any RANS turbulence model.

$$\frac{\partial}{\partial x_j}\left(\frac{\nu}{Pr}\frac{\partial T}{\partial x_j} - \overline{u_j' T'}\right) = \frac{\partial}{\partial x_j}\left[\left(\frac{\nu}{Pr} + \frac{\nu_t}{Pr_t}\right)\frac{\partial T}{\partial x_j}\right] \tag{17}$$

$$\mu_{eff} = \frac{\nu}{Pr} + \frac{\nu_t}{Pr_t} \tag{18}$$

The modifications due to the SGDH then impact the overall turbulence model purely as extra source terms in the k and τ equations and manifest only as differences in the effective viscosity.

The GGDH is a more general approach since it accounts for the interactions between shear stress and spanwise temperature gradient, as shown in Eq. (14). Because of this dependence, the diffusion coefficient in the temperature equation becomes anisotropic and is no longer accurately represented as a scalar value

$$\frac{\partial}{\partial x_j}\left(\frac{\nu}{Pr}\frac{\partial T}{\partial x_j} - \overline{u_j' T'}\right) = \frac{\partial}{\partial x_j}\left(\frac{\nu}{Pr}\frac{\partial T}{\partial x_j} + C_s \overline{u_j' u_k'}\frac{k}{\varepsilon}\frac{\partial T}{\partial x_k}\right), \tag{19}$$

and the effective viscosity is not well defined as a scalar.

Different strategies could be addressed to overcome this limitation; three of them are briefly discussed here. The first is to make the modifications in the Helmholtz solver, so it could support anisotropic diffusion coefficients. In this way all the diffusion terms could be computed fully implicitly. This approach would mostly likely result in the most robust implementation, but it requires modification to the source code. It is currently being investigated. The second strategy is to compute all the terms of the turbulent heat flux and include them as explicit source terms. This approach resulted in significant instability, however, and was deemed nonviable. The third strategy relies on a mathematical procedure in order to manage the simulation stability. It includes a strong implicit component in the turbulent heat flux, without regard to the anisotropic behavior.

$$\frac{\partial}{\partial x_j}\left(\frac{\nu}{Pr}\frac{\partial T}{\partial x_j} - \overline{u_j' T'}\right) = \frac{\partial}{\partial x_j}\left(\frac{\nu}{Pr}\frac{\partial T}{\partial x_j} + C_s ||\overline{u_j' u_k'}|| \frac{k}{\varepsilon}\frac{\partial T}{\partial x_k}\right) \tag{20}$$

This procedure results in additional "virtual" terms that are removed as explicit heat sources to compensate. This approach resulted in some instability but was successful enough to produce the results presented herein.

3.5 Future work - RANS models

Having implemented and tested the wall-resolved (i.e., resolving the thin log and viscous sublayers standard—as well as low Re versions—of the regularized $k-\omega$ and $k-\tau$ models in our Nek5000 RANS solver, in future work we plan to investigate the log-law wall-function approach based on a finite element implementation as describd in [18] In the wall function approach, we do not need very high resolution as we move the boundary to a $y+$ location of about 50–100 units away from the solid wall. The wall function approach does not need to resolve the very sharp profiles immediately adjacent to the wall. Hence, the source terms in the k and τ equations will not cause any additional stiffness or stability problems. We are currently investigating and experimenting with this approach for RANS as well as for LES, specifically for atmospheric boundary layer flows, and we plan to pursue it further in the near future.

As mentioned earlier and explained further below, we also plan to extend the $k-\tau$ version

of the RANS model implemented in Nek to support steady-state solvers in order to accelerate convergence for turbulent flows in complex geometries. We will continue to develop these solvers to make them effective for production-level simulations at scale.

4 Direct Newton Method for Steady Fluid Solvers

In the earlier studies for steady fluid problems, we investigated a Jacobian-free Newton Krylov approach where the Jacobian matrix is computed inexactly through a first-order finite difference approximation (work with PingHsuan Tsai and YuHsiang Lan). Here, as an alternative approach, we consider a direct Newton method with pressure-split preconditioning.

In this approach (work with Kento Kaneko and Paul Fischer), we used the exact Jacobian, J, for Newton's method, which entails solving a system of the form

$$Js = \text{rhs} \tag{21}$$

for the update step. The velocity update, s, must be divergence free, which can be realized by projecting the velocity onto a divergence-free field, which is available in the P_N-P_{N-2} formulation. This process can be expressed as $s = P(\hat{J})^{-1}\text{rhs}$, where $\hat{J}$ is the Jacobian for the nonlinear advection-diffusion operator and P is the projector onto the divergence-free space. We have established that P (which, as a projector, has eigenvalues 0 or 1) does not drastically alter the spectrum of $\hat{J}$. Hence, the Navier-Stokes Newton update (21) can be effectively preconditioned by an advection-diffusion preconditioner. Thus, attention to the advection-diffusion problem is warranted and has been the focus of our domain-decomposition-based approach (work with Pablo Brubeck).

Because the P_N-P_{N-2} has a well-defined projector onto a divergence-free space, this approach provides a clear path to preconditioning. We envision that once this approach is tested and validated in the P_N-P_{N-2} context, we will extend to the P_N-P_N formulation because both approaches describe the same physics, albeit through slightly different numerical formulations.

4.1 Steady Advection Diffusion

For simplicity, we begin with a formulation on a time-independent advection diffusion equation:

$$\vec{c} \cdot \nabla u \quad = k\nabla^2 u + f. \tag{22}$$

For the SEM-discretized linear equations expressed as

$$C\underline{\mathrm{u}} = -A\underline{\mathrm{u}} + B\underline{\mathrm{f}}, \tag{23}$$

we define a discrete residual function $F(\underline{\mathrm{u}}_k)$ by

$$\underline{\mathrm{F}}(\underline{\mathrm{u}}_k) = B\underline{\mathrm{f}} - C\underline{\mathrm{u}}_k - A\underline{\mathrm{u}}_k \tag{24}$$

and seek a $\underline{u}_k$ such that $\underline{F}(\underline{u}_k) \to 0$ as k increases. Introducing the Jacobian J defined as

$$J = \frac{d\underline{F}}{d\underline{u}_k} = -(C + A), \tag{25}$$

we compute the steady-state solution of (22) by Newton's method with an initial vector $\underline{u}_0$:

$$\underline{u}_1 = \underline{u}_0 - \alpha J^{-1} F(\underline{u}_0), \tag{26}$$

$$\underline{u}_{k+1} = \underline{u}_k - \alpha J^{-1} F(\underline{u}_k), \quad k = 1, \cdots, n. \tag{27}$$

4.2 Steady Navier-Stokes

For a time-independent Navier-Stokes equation, we have

$$\vec{u} \cdot \nabla \vec{u} = \frac{1}{\mathrm{Re}} \nabla^2 \vec{u} + \vec{f}, \tag{28}$$

$$\nabla \cdot \vec{u} = 0. \tag{29}$$

Then our SEM-discretized nonlinear equations can be written as

$$P_w W^{-1} \{C(\underline{u})\underline{u} = -A\underline{u} + B\underline{f}\}, \tag{30}$$

leading to a discrete residual function $F(\underline{u}_k)$ by

$$F(\underline{u}_k) = P_w W^{-1}(B\underline{f} - C(\underline{u}_k)\underline{u}_k - A\underline{u}_k), \tag{31}$$

where P_w is a projection onto the closest divergence-free velocity. Then we seek a $\underline{u}_k$ such that $\underline{F}(\underline{u}_k) \to 0$ as k increases. Defining J by

$$J(\underline{u}_k) = \frac{d\underline{F}}{d\underline{u}_k}, \tag{32}$$

$$= -P_w W^{-1}(C(\underline{u}_k) + C'\underline{u}_k + A), \tag{33}$$

the Jacobian matrix can be written in block form

$$J(\vec{\underline{u}}) = \left[\frac{d\underline{F}}{d\underline{u}} \frac{d\underline{F}}{d\underline{v}}\right] \tag{34}$$

$$= P_w(I \otimes W^{-1}) \begin{bmatrix} A + C(\underline{u}, \underline{v}) + C(\cdot, \underline{0})\underline{u} & C(\underline{0}, \cdot)\underline{u} \\ C(\cdot, \underline{0})\underline{v} & A + C(\underline{u}, \underline{v}) + C(\underline{0}, \cdot)\underline{v} \end{bmatrix}, \tag{35}$$

where the convective term is nonlinear, the Jacobian matrix is dependent on the current solution $\underline{u}_k$, and C' is a rank-3 tensor. Therefore, the Jacobian applied to an arbitrary vector $\vec{\underline{s}}$ is

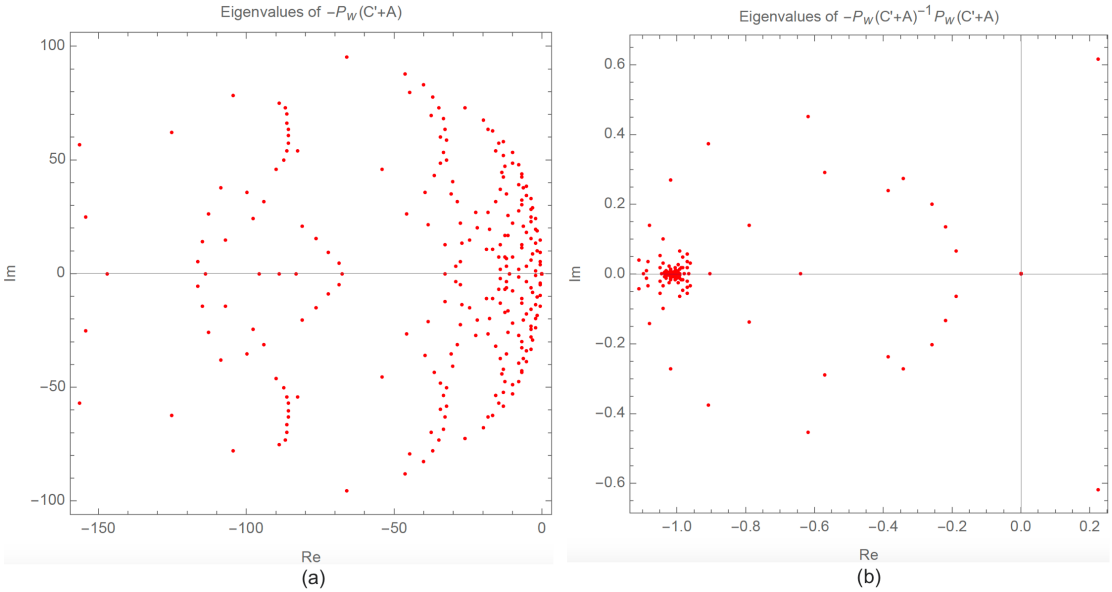

Figure 18: Eigenvalue spectrums of $-P_w(C'+A)$ and $-P_w(C'+A)^{-1}P_w(C'+A)$.

$$J(\vec{\underline{u}})\,\vec{\underline{s}} = P_w(I\otimes W^{-1})\begin{bmatrix}(A+C(\underline{u},\underline{v}))\underline{s}_1+C(\underline{s}_1,\underline{0})\underline{u}+C(\underline{0},\underline{s}_2)\underline{u}\\ C(\underline{s}_1,\underline{0})\underline{v}+(A+C(\underline{u},\underline{v}))\underline{s}_2+C(\underline{0},\underline{s}_2)\underline{v}\end{bmatrix} \tag{36}$$

$$= P_w(I\otimes W^{-1})\begin{bmatrix}(A+C(\underline{u},\underline{v}))\underline{s}_1+C(\underline{s}_1,\underline{s}_2)\underline{u}\\ (A+C(\underline{u},\underline{v}))\underline{s}_2+C(\underline{s}_1,\underline{s}_2)\underline{v}\end{bmatrix}. \tag{37}$$

Figures 18 (a)–(b) demonstrate the spectrum of eigenvalues for $-P_w(C'+A)$, scattered in the negative half-plane in the range of $[-150,0]\times[-100,100]$, and the spectrum of eigenvalues for a proposed preconditioned system $-P_w(C'+A)^{-1}P_w(C'+A)$, clustered around $(-1,0)$, which would give the potential to reduce the iteration count. We also examined the eigenspectrums with and without the divergence-free projection per iteration, demonstrating no difference, and thus concluded that projection in each GMRES iteration during the Newton procedure is unnecessary, thus saving costs.

Figures 19 (a)–(c) demonstrate the steady solution of the lid-driven cavity problem for Reynolds numbers of 1000, 5000, and 10000, obtained by the direct Newton method. Without preconditioning, the iteration counts per Newton step are larger than 300. As future work, a preconditioning strategy using the tensor-product-based fast diagonalization on the advection-diffusion operator will be considered for solving (21), which can be applied for both the direct Newton and Jacobian-Free Newton Krylov methods.

In summary, the algorithmic development of steady-state solvers would require a long-term effort for the following components with a major push in the effective preconditioners:

- Develop a nonsymmetric coarse grid solver.

- Develop a steady advection-diffusion preconditioner to our direct Newton method for solving steady Navier-Stokes problems.
- Develop a steady advection diffusion preconditioner to our Jacobian-Free Newton Krylov method for solving steady Navier-Stokes problems.
- Develop a steady advection-diffusion preconditioner to our Jacobian-Free Newton Krylov method for solving Reynolds-averaged Navier-Stokes problems.
- Develop a nonsymmetric algebraic multigrid solver using the approach by James Lottes (2015).

4.3 High-Performance Computing Effort

The ECP ANL/CEED team has made a significant advance in software development in order to support NEAMS problems running at large scale on advanced computing architectures [19]. NekRS, a GPU variant of Nek5000, was built on top of kernels from libParanumal using OCCA for portability. On a CPU platform, Nek5000 strong-scales up to only one or two spectral elements per MPI rank. On GPUs such as the NVIDIA V100, it requires about 2 million gridpoints per V100 for reasonable efficiency. Strong- and weak-scaling performances for NekRS and Nek5000 on Summit have been achieved, including a full-core mesh consisting of 37 of 17×17 rod bundles, with 174 millon spectral elements (total 59 billon grid points using 7th-order approximations) running on the full system of Summit (4,608 nodes, 27,648 GPUs).

The most recent performance enhancements in NekRS, including communication overlap and improved preconditioners, achieve time per step less than 0.1 seconds for the full-core flow simulations. Ongoing collaboration between NEAMS and CEED teams at Argonne include Voroni cell-based all-hex meshing for pebble-bed reactors (currently supporting up to 50,000 pebbles at a low element count using ∼300 spectral elements per pebble), preconditioning strategies for pressure solve, and portable and scalable software development for existing advanced architectures and upcoming exascale machines for thermal-hydrualic simulations.

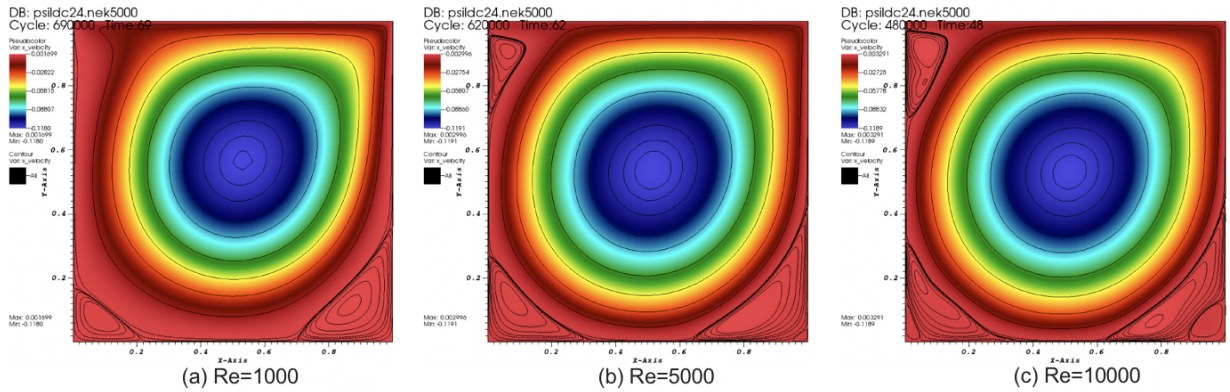

(a) Re=1000 (b) Re=5000 (c) Re=10000

Figure 19: Steady solution by the direct Newton method for lid-driven cavity problems.

5 Summary and Future Work

This year, the the Nuclear Energy Advanced Modeling Simulation program (NEAMS) thermal-hydraulics verification and validation (V&V) work has focused on the following Nek5000 V&V-driven development.

First, we have continued assisting the U.S. NRC staff with Nek5000 setups and validation for a range of problems relevant to and including the HYMERES-2 benchmark currently carried out in the PSI PANDA facility. The primary focus of this year's efforts of the ANL-NRC collaboration on benchmark modeling resulted in more efficient geometry and inlet modeling simplification after a careful study of the inlet sensitivity solutions. This modeling choice significantly simplifies the next step of the cross-V&V HYMERES-2 project where the heat and mass transfer solution will be obtained and compared. In addition, the ANL team continue to provide assistance to the NRC staff in the form of Nek5000 application support in general and on HPC platforms of ALCF and INL in particular, during the NRC's assessment of the solver usage for exploratory parameter, reference, and closure simulations being a part of NRC Blue CRAB code suite.

Second, we have implemented and tested a more robust model of URANS, namely a $k-\tau$ model, a variant of the $k-\omega$ model, along with other improvements to RANS Nek5000 modeling in general. Because of its demonstrated robustness and stability, the $k-\tau$ model is the only RANS model that has been implemented in the new GPU version of the Nek5000 code, nekRS. Efforts in the coming year will be focused on implementing wall models and an evaluation of other RANS models, such as $k-\varepsilon$.

Finally, we report on the initial implementation of Jacobian-free Newton Krylov approach to the direct Newton method for steady fluid solvers aimed at acceleration of RANS modeling and at IC improvement for LES campaigns. We have established the necessity of subsequent algorithmic development for a range of components to increase the efficiency of its preconditioners. Also leveraging the ECP ANL/CEED and SMR teams' software development effort to support NEAMS problems at large scale on the advanced computing architectures, NekRS, a GPU variant of Nek5000, built on top of kernels from libParanumal using OCCA for portability, has been successfully run on the full system of Summit (4,608 nodes, 27,648 GPUs).

Acknowledgments

Argonne National Laboratory's work was supported by the U.S. Department of Energy, Office of Nuclear Energy, Nuclear Energy Advanced Modeling and Simulation (NEAMS) program, under contract DE-AC02-06CH11357.

We acknowledge the use of computing resources provided by the INCITE and ASCR Leadership Computing Challenge (ALCC) programs at the Argonne Leadership Computing Facility (ALCF) and local computing resources provided by the NSE Division of Argonne National Laboratory.

This research made use of Idaho National Laboratory computing resources which are supported

by the Office of Nuclear Energy of the U.S. Department of Energy and the Nuclear Science User Facilities under Contract No. DE-AC07-05ID14517.

We thank Gail Pieper for editing the manuscript.

References

[1] *Nek5000 Version 19.0.* December, 2019. Argonne National Laboratory, Argonne, Illinois. Available: https://nek5000.mcs.anl.gov.

[2] A. Obabko, E. Merzari, P. F. Fischer, S. M. Aithal, and A. Tomboulides, "Large-eddy simulations of stratification layer erosion by a jet," in *67th Annual Meeting of the APS Division of Fluid Dynamics*, vol. 59 (20) of *Bulletin of the American Physical Society*, (San Francisco, CA), Nov. 2014.

[3] A. Kraus, S. Aithal, A. Obabko, E. Merzari, A. Tomboulides, and P. Fischer, "Erosion of a large-scale gaseous stratified layer by a turbulent jet simulations with URANS and LES approaches," in *Int. Conf. on Nuclear Reactor Thermal Hydraulics (NURETH-16)*, (Chicago, IL), Sept. 2015.

[4] A. Tomboulides, S. M. Aithal, P. F. Fischer, E. Merzari, A. V. Obabko, and D. R. Shaver, "A novel numerical treatment of the near-wall regions in the $k - \omega$ class of RANS models," *International Journal of Heat and Fluid Flow*, vol. 72, pp. 186–199, 2018.

[5] G. Kalitzin, A. Gould, and J. Benton, "Application of two-equation turbulence models in aircraft design," *AAIA*, vol. 96, p. 0327, 1996.

[6] G. Medic, J. A. Templeton, and G. Kalitzin, "A formulation for near-wall RANS/LES coupling," *International Journal of Engineering Science*, vol. 44, pp. 1099–1112, 2006.

[7] A. Obabko, P. Fischer, O. Marin, E. Merzari, and D. Pointer, "Verification and validation of Nek5000 for T-Junction, Matis, SIBERIA, and Max experiments," in *Int. Conf. on Nuclear Reactor Thermal Hydraulics (NURETH-16)*, (Chicago, IL), Sept. 2015.

[8] D. Wilcox, *Turbulence Modeling for CFD.* La Cañada, CA: DCW Industries, 1998.

[9] D. Wilcox, "Formulation of the k-ω turbulence model revisited," *AAIA Journal*, vol. 46, no. 11, pp. 2823–2838, 2008.

[10] A. Tomboulides, S. M. Aithal, P. F. Fischer, E. Merzari, and A. V. Obabko, "Initial implementation of uRANS k-omega standard, regularized and regularized SST model in Nek5000 module," Tech. Rep. ANL/MCS-TM-335, Argonne National Laboratory, July 2013.

[11] A. Tomboulides, S. M. Aithal, P. F. Fischer, E. Merzari, and A. V. Obabko, "A novel variant of the k-ω urans model for spectral element methods - implementation, verification and validation

in Nek5000," in *ASME 2014 4th Joint US-European Fluids Engineering Division Summer Meeting*, vol. 1D of *ASME Proceedings, FEDSM2014-21926*, (Chicago, IL), Aug. 2014.

[12] J. Kok and S. Spekreijse, "Efficient and accurate implementation of the k-ω turbulence model in the NLR multi-block Navier-Stokes system," Tech. Rep. NLR-TP-2000-144, National Aerospace Laboratory, 2000.

[13] S. Jovic and D. Driver, "Backward-facing step measurements at low Reynolds number, Re=5000," Tech. Rep. 108807, NASA Technical Memorandum, 1994.

[14] C. L. Ladson, "Effects of independent variation of mach and reynolds numbers on the low-speed aerodynamic characteristics of the naca 0012 airfoil section," Tech. Rep. NASA-TM-4074, L-16472, NAS 1.15:4074, NASA Langley Research Center, Hampton, VA, United States, 1988.

[15] K. J. Hsieh and F. S. Lien, "Numerical modeling of buoyancy driven turbulent flows in enclosures," *International Journal of Heat and Fluid Flow*, vol. 25, pp. 659–670, 2004.

[16] F. Ampofo and G. Karayiannis, "Experimental benchmark data for turbulent natural convection in an air-filled squared cavity," *International Journal of Heat and Mass Transfer*, vol. 46, pp. 3551–3572, 2003.

[17] S. Kenjeres and K. Hanjalic, "Prediction of turbulent thermal convection in concentric and eccentric horizontal annuli," *International Journal of Heat and Fluid Flow*, vol. 16, pp. 429–439, 1995.

[18] O. Kuzman, S. Mierka, and S. Turek, "On the implementation of the k-ω turbulence model in incompressible flow solvers based on a finite element discretisation," *International Journal of Computing Science and Mathematics archive*, vol. 1, pp. 193–206, 2007.

[19] E. Merzari, J. Fang, D. Shaver, M. Misun, P. Fischer, Y.-H. Lan, R. Rahaman, and P. Romano, "Initial full core SMR simulations with NekRS," Tech. Rep. ADSE08-105, Exascale Computing Project, 2020.

Nuclear Science and Engineering Division
Argonne National Laboratory
9700 South Cass Avenue, Bldg. 208
Argonne, IL 60439

www.anl.gov